Application of the tilt derivative transform to bathymetric data for structural lineament mapping

Christopher Mark Yeomans[1], Matthew Head[1], Jordan James Lindsay[1]

[1]Camborne School of Mines, College of Engineering, Mathematics and Physical Sciences, University of Exeter, Penryn Campus, Penryn, Cornwall, TR10 9FE, UK

Key Points:

- High-resolution bathymetric data are used to analyse submerged outcrops for structural lineaments
- Steps in bathymetry cause problems when enhancing lineaments using common feature extraction methods
- The tilt derivative transform successfully enhances lineaments prior to lineament extraction

Corresponding author: Christopher M Yeomans, `c.m.yeomans@exeter.ac.uk`

Abstract

High-resolution bathymetry surveys provide an opportunity to analyse local geological structure where onshore areas afford limited exposure. Semi-automated lineament detection methods are necessary for areas of large coverage where a manual analysis would be subjective and time-consuming. However, semi-automated approaches are dependent on effective feature extraction methods to identify all lineaments. This letter illustrates some the problems that can impede some processing methods where sharp steps in the seafloor (e.g. palaeocoastlines) are present. Directional gradient, Sobel and Laplacian filters are explored as well as the hillshade and tilt derivative transform for feature extraction prior to applying an object-based image analysis lineament detection approach. The filtered datasets generally perform poorly with a marked improvement when using the hillshade transform. However, it is the azimuth-invariant tilt derivative, which incorporates a convolved vertical derivative, that is most successful, identifying lineaments in a range of orientations and across a sharp step in the seafloor.

Plain Language Summary

Spatial patterns of lineaments can provide information about fracture networks in bedrock which is important for understanding tectonic evolution, fluid flow and mineralisation among other geological phenomenon. Detailed measurements of the topography of the seafloor coupled with careful use of image enhancement techniques can help the visual representation of bedrock structures. These can then be extracted through a semi-automatic process which saves time and limits potential bias in the analysis. This is difficult in areas with sharp changes in the height of the seafloor. Our study highlights the capability of the tilt derivative transform to produce clear lineament maps that retain detail across changes in seafloor depth. Processing the data in this way is an important step for an effective analysis and maximise significant results. The results of this study will allow for more efficient analysis of larger offshore areas to enhance our understanding of the regional geology.

1 Introduction

The bathymetry of the seafloor is complementary to the topography of the land and can describe various morphological features in the marine environment such as sedimentary bedforms or submerged outcrop (Hell et al., 2012). These data produce a continuous surface of the seabed and provide an excellent means for viewing the structural complexity of exposed bedrock (Collier et al., 2006; Nixon et al., 2012). High-resolution data are particularly effective at defining areas of submerged outcrop and capture the detail of geological structure including bedding of strata and cross-cutting faults where these features dip $>10°$ (Collier et al., 2006). Bathymetric data has also been shown to enhance the interpretation of seismic reflection data to better understand the geometry of structures and stratigraphy (Collier et al., 2006; Sanderson et al., 2017; Westhead et al., 2018).

Bathymetric data has been employed in a variety of studies to map geological structure and to enhance the interpretation of seismic reflection data (e.g. Collier et al., 2006; Nixon et al., 2012; Sanderson et al., 2017; Westhead et al., 2018). By remotely mapping seafloor lineaments, the structural evolution of an area can be defined. Where submerged outcrop can be identified, high-resolution bathymetric data can provide an excellent input dataset for lineament detection. The data capture the detail of geological structure including bedding of strata and cross-cutting faults where these features dip $>10°$ (Collier et al., 2006). The extensive coverage, often at high-resolution, available for these studies require a semi-automated lineament detection method and increase the objectivity of the analysis. Therefore, prior feature extraction as part of a semi-automated approach is key for mapping offshore lineaments.

This study investigates the effectiveness of different operators as a means for feature extraction, including directional gradient and Sobel filters, azimuth-invariant Laplacian filters as well as transforms such as hillshading and the tilt derivative (TDR). The study uses bathymetric data from SW England over a classic area of offshore NW Devon, illustrated in Figure 1 and utilises a state-of-the-art Object-based Image Analysis (OBIA) lineament detection method designed by Yeomans et al. (2019). A small subset of the study area over the platform edge is highlighted in this letter; full analyses are included in the Supplementary Information.

Understanding how different filters and transforms affect the final lineament population is important for selecting the most appropriate feature extraction tool when applying semi-automated methods. The different visualisations tested here test the importance of not only weighting azimuth equally but also examines how vertical changes in bathymetry can affect the results. The study forms a precursor prior to lineament detection and structural analysis of offshore areas at a regional scale.

1.1 Geological setting

The geology of the study area comprises Culm Basin rocks which were deformed during Variscan orogenesis creating gently plunging chevron folds and predominantly NNW-directed thrusts (Rattey & Sanderson, 1984; Holder & Leveridge, 1986; Lloyd & Chinnery, 2002; Leveridge & Hartley, 2006). During this time, strike-slip transfer faults were formed in a NW to NNW orientation (Leveridge et al., 2002). The breakup of Pangaea brought about subsequent phases of extension during the Mesozoic and later Alpine collision caused minor inversion and substantial Cenozoic strike-slip movement (Holloway & Chadwick, 1986; Cheadle et al., 1987; Chapman, 1989; Hillis et al., 2008). These NW-SE structures, and subordinate NE-SW structures, have been reactivated multiple times during this period (Shail & Alexander, 1997; Ault et al., 2016), and have previously been investigated by Nixon et al. (2012) and Nyberg et al. (2018). They form the target for semi-automated lineament detection in this study and are of particular importance for understanding the post-Variscan structural evolution of the region.

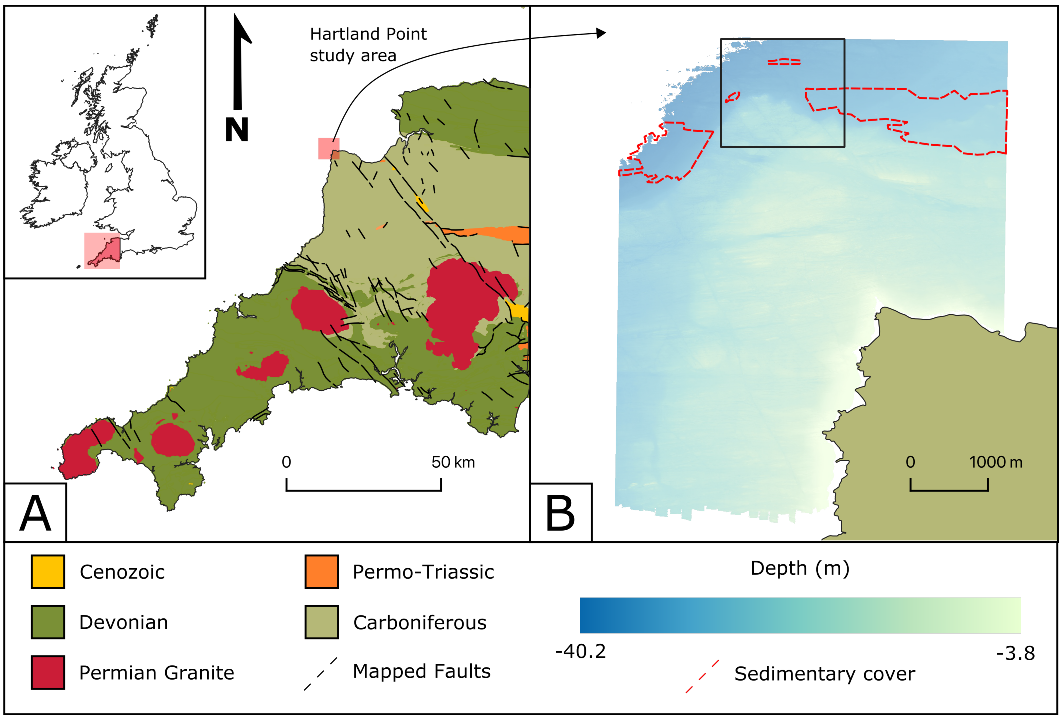

Figure 1. A) Regional overview of the study area, detailing the primary geological units in SW England B) Seafloor depth off of Hartland Point, with the rectangle highlighting an area that contains a step-change in bathymetry (reflecting a palaeocoastline) used to showcase the feature extraction methods and resulting lineament populations. Geology based upon BGS Geology 625k (DiGMapGB-625) data, with the permission of the British Geological Survey.

2 Data and methods

Manual lineament extraction studies can be effective at identifying structural features and creating maps of fault systems (e.g. Nixon et al., 2012). These studies often produce maps with long lineament traces that appear robust but can be subjective and dependent on the data visualisation (Scheiber et al., 2015). Biases can exist in various aspects of a manual analysis including lineament length and the scale/detail of fractures mapped, although user experience appears to be less important (Andrews et al., 2019). Semi-automated methods can mitigate these biases but the data often still require enhancement via feature extraction methods; thus requiring careful consideration. Directional filters such as gradient and Sobel kernels are effective at finding lineaments where the orientation is known; the same holds for the hillshade transform. Where this is not the case, the method must be azimuth-invariant and give all lineaments in the $X-Y$ plane equal weight (e.g. Laplacian filters). Changes in the vertical plane can also influence the outputs, which is why the tilt derivative (TDR) transform is investigated in this study and compared to the aforementioned filters and hillshade transform.

2.1 Bathymetric data

The area of interest selected for this study is in the region offshore of Hartland Point, Devon (Figure 1b). Bathymetric data were downloaded at 2 m pixel resolution from the United Kingdom Hydrographic Office (UKHO) via the Admiralty Data Portal; full details can be found in Supplemtary Data. The site covers an area of submerged outcrop with a distinct platform area curtailed to the north of the study by an apparent palaeocoastline. This on-platform area extends some 2800 m west of the present coastline with a gentle gradient into deeper off-platform areas whereas to the north the on-platform area extends approximately 2300 m where a sharp drop >10 metres in the platform occurs over a palaeocoastline. Although sand cover becomes problematic in the westernmost part of the area, it is largely limited to the nearshore coves with small pockets found along the palaeocoast. The area was featured as part of a manual lineament analysis by Nixon et al. (2012) who determined a series of NW-SE and NE-SW trending fault sets that showed dextral and sinistral offsets, respectively. The area is also used as a case study site to showcase the NetworkGT plug-in for QGIS software, which consists of a suite of tools for geometric and topological analysis of two-dimensional fracture networks (Nyberg et al., 2018). Both Nixon et al. (2012) and Nyberg et al. (2018) have demonstrated that the area provides an excellent site for studying the fault networks and this study will aim to extend this into deeper water.

2.2 Filters and transforms

Geospatial data, even after all processing steps have been completed, almost always require some further manipulation to enhance certain features prior to further analysis; for image or raster data, this often involves a filter or transform. There are a broad range of enhancements that can be tailored to the task and, when used with an appropriate semi-automated algorithm, a high degree of accuracy can be achieved (Sukumar et al., 2014). However, determining a "good" image enhancement can be difficult and potentially subjective especially depending on the target structure and the signal-to-noise ratio (Smith & Clark, 2005; Rahnama & Gloaguen, 2014).

Band pass filters, such as the gradient and Sobel operators, are effective at selecting a particular range (based on directionality) whereas Laplacian filters are azimuth-invariant. Low-pass and high-pass filters are useful for mitigating noise and enhancing the sharpness of features, respectively (Rahnama & Gloaguen, 2014). Transforms do not preferentially select data but convert the whole dataset to derive a new variable. In this study, the directional gradient, Sobel and Laplacian filters as well as the hillshade and TDR transforms have been selected to demonstrate various feature extraction methods.

It is worth noting that the use of directional filtering has become less popular over time due to the availability of more rigorous algorithms (Airo, 2013). The ability to semi-automate lineament extraction and loop through a range of azimuths has meant that more objective lineament maps can be created compared to using weights oriented along an arbitrary compass direction (e.g. Rahnama & Gloaguen, 2014; Middleton et al., 2015; Šilhavý et al., 2016; Yeomans et al., 2019). However, many studies still implement the use of directional filters as a first pass for lineament mapping (Mallast et al., 2011; Sedrette & Rebaï, 2016).

2.2.1 Directional filters

Directional filtering of spatial data is a well-established tool used to highlight features for lineament detection and structural mapping. The filter uses a weighted kernel to accentuate particular-oriented features, where features are perpendicular to the overall gradient of weights within the kernel. The use of directional filters was detailed by Moore and Waltz (1983) who provided a five-step framework for lineament enhancement that included smoothing, directional filtering, smoothing directional components, lineament extraction and scaling. The process takes the focal pixel, A_0, and surrounding pixels $(B, C...I)$ from the input data λ in Equation 1:

$$\lambda = \begin{bmatrix} B & C & D \\ E & A_0 & F \\ G & H & I \end{bmatrix} \tag{1}$$

The values in λ are convolved by a directional kernel in Equation 2 containing, in this case, a northwest gradient:

$$G_{NW} = \begin{bmatrix} -2 & -1 & 0 \\ -1 & 0 & 1 \\ 0 & 1 & 2 \end{bmatrix} * \lambda \tag{2}$$

or a northeast gradient using Equation 3:

$$G_{NE} = \begin{bmatrix} 0 & -1 & -2 \\ 1 & 0 & -1 \\ 2 & 1 & 0 \end{bmatrix} * \lambda \tag{3}$$

The results of these orthogonal filters can be combined as a magnitude using Equation 4:

$$|G| = \sqrt{G_{NW}^2 + G_{NE}^2} \tag{4}$$

The weights used here have been chosen to emphasise the main directions of known faults in the study area. However, directional filtering can vary considerably depending on the task in hand, but generally take the form of a 3 x 3 kernel where the direction of positive-to-negative weighting provides the orientation of the kernel.

2.2.2 Sobel filter

The Sobel filter is a commonly used edge detector technique and allows the calculation of the X and Y derivatives with a level of smoothing imparted via the kernel (Sobel & Feldman, 1973; Favalli & Fornaciai, 2017). It is another directional gradient-based method where the X and Y derivatives for the Sobel filter are calculated using Equation 5 and Equation 6, respectively.

$$G_H = \begin{bmatrix} 1 & 0 & -1 \\ 2 & 0 & -2 \\ 1 & 0 & -1 \end{bmatrix} * \lambda \tag{5}$$

$$G_V = \begin{bmatrix} 1 & 2 & 1 \\ 0 & 0 & 0 \\ -1 & -2 & -1 \end{bmatrix} * \lambda \tag{6}$$

These two first-order derivatives can then be combined into a gradient magnitude image using Equation 7:

$$|G| = \sqrt{G_H^2 + G_V^2} \tag{7}$$

The Sobel filter is most sensitive to lineaments in the X and Y directions and diagonal components can be suppressed (Sobel & Feldman, 1973). The Sobel filter is essentially a modification of the Prewitt filter which does not account for smoothing. The introduction of a -2 weight to the filter (compared to a -1 for the Prewitt filter) adds a more 'circular' operation to the kernel that is advantageous over the Prewitt filter (Davies, 1986).

2.2.3 Laplacian filter

The Laplacian filter is a second-order derivative, non-directional filtering tool that has been widely applied for detecting structural lineaments from remotely sensed data (e.g. Grebby et al., 2012; Rahnama & Gloaguen, 2014; Al-Azemi & Divi, 2017). The Laplacian can be derived using Equation 8, which can be approximated by convolving the matrices described in Equation 9 and Equation 10 for a 3 x 3 kernel and 5 x 5 kernel, respectively.

$$L_{(x,y)} = \nabla^2 f_{(x,y)} = \frac{\delta^2 f(x,y)}{\delta x^2} + \frac{\delta^2 f(x,y)}{\delta y^2} \tag{8}$$

$$L_{(3)} = \begin{bmatrix} 0 & -1 & 0 \\ -1 & 4 & -1 \\ 0 & -1 & 0 \end{bmatrix} * \lambda \tag{9}$$

$$L_{(5)} = \begin{bmatrix} 0 & 0 & -1 & 0 & 0 \\ 0 & -1 & -2 & -1 & 0 \\ -1 & -2 & 17 & -2 & -1 \\ 0 & -1 & -2 & -1 & 0 \\ 0 & 0 & -1 & 0 & 0 \end{bmatrix} * \lambda \tag{10}$$

The Laplacian filter is useful as it returns a smoother image where edges are located at the zero-contour (Marr & Hildreth, 1980). Being a second-order derivative, the Laplacian filter is more sensitive to noise in the data and may also be prone to edge-effects in the data (Maini & Aggarwal, 2009). Other derivations of the filter can mitigate this by combining Gaussian smoothing to enhance edge detection (e.g. Maini & Aggarwal, 2009; Rahnama & Gloaguen, 2014).

2.2.4 Hillshade transform

A shaded relief, or hillshade transformation, is a common tool for visualising topographic data and a useful first step for lineament mapping (Höfle & Rutzinger, 2011;

Scheiber et al., 2015; Favalli & Fornaciai, 2017). It involves transforming a 2D image to highlight features in a particular direction based on a theoretical sun position; assuming a Lambertian surface and single light source at an infinite distance (Favalli & Fornaciai, 2017). The sun position is defined by an *azimuth* (A_s) and *zenith* (Z_s) and is combined with a *slope* (S_e) and *aspect* (A_e) derived from the elevation model to calculate the hillshade (H) image (Equation 11) where all all angles are converted to radians.

$$H = 255 * ((\cos(Z_s) * \cos(S_e)) + (\sin(Z_s) * \sin(S_e) * \cos(A_s - A_e))) \tag{11}$$

Shadows are imparted on the image based on the azimuth and zenith of the light source where a zenith of zero would place the sun on the horizontal plane of reference. The single light source results in azimuth biasing and can change the apparent position of breaks in slope as well as the apparent convexity or concavity of a feature (Smith & Clark, 2005; Favalli & Fornaciai, 2017). This can be mitigated by using multiple hillshade images where at least two images are generated parallel, and orthogonal, to the principal lineament orientation to capture the main trends (Smith & Clark, 2005). This approach is similar to the methods of directional filters but is not limited to orientations in the X and Y directions of the image. Additionally, lower zenith angles and the linearly normalised range of 0-255 can lead to a loss of detail in areas of extremely prominent topography.

2.2.5 Tilt derivative transform

The tilt derivative (TDR) transform was first described by Miller and Singh (1994) whereby a tilt angle is determined by the arctangent of the vertical and total horizontal derivative of the data (T) (Equation 12). The transform was developed for use with potential field data, primarily magnetic data, but has since been applied to other datasets such as LiDAR data (Middleton et al., 2015) and the Total Count of radiometric data (Yeomans et al., 2019) where the vertical derivative is calculated through convolution.

$$TDR = \tan^{-1}\left(\frac{\dfrac{\partial T}{\partial z}}{\sqrt{\left(\dfrac{\partial T}{\partial x}\right)^2 + \left(\dfrac{\partial T}{\partial y}\right)^2}}\right) \tag{12}$$

The TDR transform is a useful tool for preserving low amplitude signals which may be attenuated over the dynamic range in the presence of a larger amplitude signal (Miller & Singh, 1994; Verduzco et al., 2004; Fairhead et al., 2004). Values are restricted to $\pm\pi/2$ by the arctangent function, regardless of the derivative magnitudes, preserving low amplitude signals and reducing the effect of noise. Additionally, this feature assists the interpretation where the continuity of a body may vary due to lateral changes in signal (Verduzco et al., 2004). Furthermore, the zero-contour passes over or near the edge of bodies (Miller & Singh, 1994). These features make the TDR transform an effective tool for mapping edges or mapping minima/maxima.

2.3 Lineament detection using OBIA

Lineament detection techniques have commonly taken a pixel-based approach to feature identification. The results have shown broad improvement over several decades but are still fallible in noisy data and in areas where lineaments appear discontinuous. Object-Based Image Analysis (OBIA) workflows allow the generation of spatially correlated groups of pixels or "image objects" to identify lineaments. The advantage of an OBIA approach is that objects have internal and relative statistics as well as a geospatial topology that can hone the classification (Lang, 2008). The use of these attributes can result in a more subjective approach (Blaschke et al., 2004) but the analysis is more robust to noise compared to pixel-based methods (Van Den Eeckhaut et al., 2005, 2012). Image objects have proven an effective means for lineament detection and used on a variety of data types including spaceborne InSAR and Landsat data (Mavrantza & Argialas, 2006; Marpu et al., 2008), as well as airborne LiDAR, magnetic and radiometric data (Rutzinger et al., 2006; Middleton et al., 2015; Yeomans et al., 2019).

Herein, an OBIA workflow is used to capture lineaments in the bathymetry. Prior to the analysis, outliers were removed and the ranges for each filter and the hillside transform were linearly transformed to optimise performance within the algorithm; see Supplementary Information. The data are taken as a single input layer using the bottom-up OBIA method described by Yeomans et al. (2019). The method efficiently performs lineament extraction from large raster datasets whilst creating slightly shorter lineament segments compared to top-down OBIA methods (e.g. Middleton et al., 2015; Yeomans et al., 2019). For this study, line extraction was completed in two phases and optimised for each data input. The first phase searched for NW-SE lineaments using a line width of 5 pixels for the TDR transform and 2 pixels for the other data inputs, the second phase targeted NE-SW lineaments with a line width of 2 pixels for the TDR transform and 1 pixel for all other data. The resultant image objects were then merged and processed as per the approach outlined in Yeomans et al. (2019).

3 Results and discussion

In this section, we present visualisations using each of the filters and transforms introduced above and the subsequent derived lineaments. The semi-automated OBIA approach to lineament detection ensures an objective interpretation between different visualisations of the data.

3.1 Data visualisation

The operations performed on the data are presented in Figure 2, over the zoomed area (illustrated in Figure 1b). The zoomed area shows the edge of the platform and provides a good comparison of how the filters and transforms perform across this pronounced change in depth. It can be seen from Figure 2a that the magnitude of the gradient filter is effective at dealing with the sharp break in the data but by its nature tends toward highlighting the edges of submerged outcrop blocks, rather than identifying fractures in the bedrock. Similarly, the magnitude of the Sobel filter in Figure 2b captures edges of blocks and is not well suited to define minima. Although the filtered data range appears to be better at recognising structure in the off-platform data, it is oversaturated on the platform resulting in an apparent loss of resolution.

Compared to the previous filters, the Laplacian filter produces a smoother visualisation of the data. The 3 x 3 kernel shown in Figure 2c provides a slight enhancement on the data to highlight structures but is overall indistinct at this scale and appears to have greater noise. The 5 x 5 kernel (Figure 2d) emphasises more structures in both on-platform and off-platform areas whilst reducing noise to give a sharper image.

Figure 2e and 2f show the data following the hillshade and tilt derivative transforms, respectfully. The hillshaded image, which uses an illumination azimuth of 225° and zenith of 45°, clearly detects the NW-SE in the on-platform areas of the seafloor but struggles to highlight such detail in the deeper off-platform areas. The tilt derivative provides a more complete picture where structures are equally apparent despite the step-change in platform height over the area. The use of a total horizontal derivative in the denominator means that there is no azimuthal bias to highlight particular orientations of lineaments in the data, as is the case with the hillshade transform.

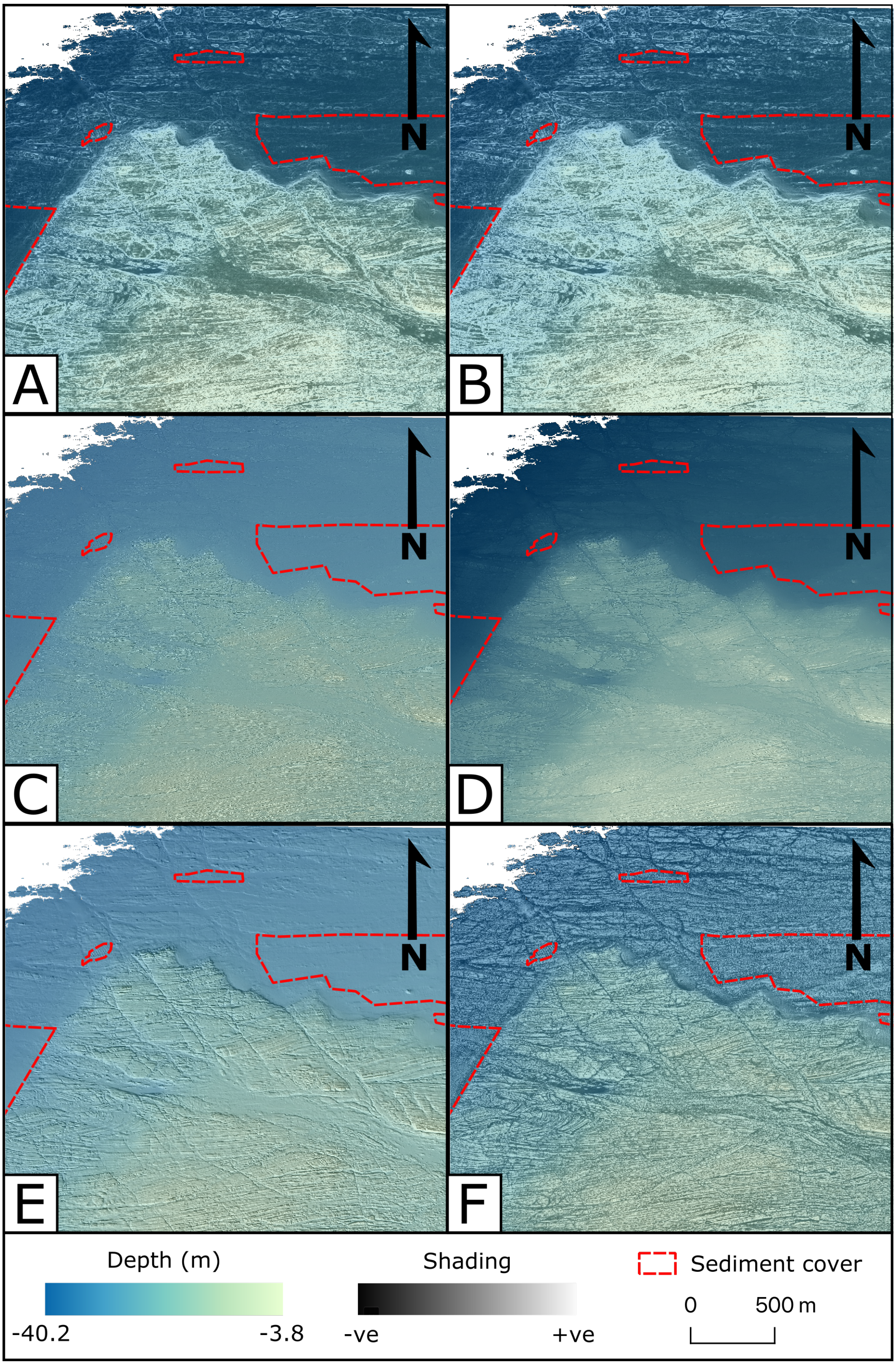

Figure 2. Zoomed area used to showcase different feature extraction methods used in this study. A) magnitude of gradient filter; B) magnitude of Sobel filter; C) 3 x 3 Laplacian filter; D) 5 x 5 Laplacian filter; E) hillshade transform; F) tilt derivative (TDR) transform.

3.2 Lineament populations

A subset of the derived lineaments, shown in Figure 3, highlight the performance of each operator from on-platform to off-platform areas, where the water depth increases >10 metres. The off-platform area has some sedimentary cover causing low-quality data but does display NW-SE structures that correlate with on-platform structures. Full figures of the lineament populations across the whole study area are provided in the Supplementary Information.

The number of lineaments derived from gradient-filtered data across Zone 1 is not substantial, with the majority of lineaments found over on-platform areas. Figure 3a weakly defines some NW-SE features in the data but the lack of contiguous segments make interpretation more difficult. The off-platform areas perform even more poorly and this is likely a function of the lack of smoothing (as mentioned for Zone 2) but also the more subtle features in off-platform areas being masked by the significant gradient caused across the step in the seafloor. In Figure 3b, lineaments derived from Sobel-filtered data show a reasonable level of detail in the on-platform areas although continuous features are difficult to observe. The off-platform areas are an improvement with respect to the gradient methods but also lack easily identifiable structures. Despite the smoothing component incorporated into the Sobel kernels, these off-platform lineaments remain elusive.

Lineaments derived from Laplacian-filtered data show reasonable on-platform features. The 3 x 3 kernel (Figure 3c) identifies an abundance of short lineaments, although these produce short segments that do not easily define NW-SE or NE-SW trending structures. The off-platform lineaments appear to be largely a function of noise, not giving clear definition to any features. In contrast, the 5 x 5 kernel (Figure 3d) produces a less noisy lineament population and longer lineament segments, clearly defining some key structures in Zone 1. The off-platform areas, however, do not display any distinguishable features. The interpretation that the 5 x 5 kernel has been effective at suppressing noisy lineaments further suggests off-platform lineaments detected using data filtered by the 3 x 3 kernel are spurious.

A vast population of lineaments across the on-platform area has been generated from the hillshade-transformed data (Figure 3e), despite only identifying NW-SE features due to the azimuth of illumination. Major structures are clearly identified and are traceable with long segment lengths to the lineaments. The population also contains a signifiant amount of small lineaments which appear to be more robust when compared with the noisier populations seen in Figure 3c from the 3 x 3 Laplacian filter. However, the off-platform area underperforms, showing few lineaments and many of those that are detected do not have contiguous segments. In contrast, lineaments derived from the TDR-transformed data show clear structures, albeit with fewer short segments in some areas (Figure 3f). The lineaments detected define clear NW-SE trending features in on-platform areas and also identify some subordinate NE-SW structures. Importantly, the off-platform areas show an abundance of lineaments, which present contiguous segments, and are traceable back to on-platform features; although, many are generated in areas of sediment cover which could be the result of amplified noise.

3.3 Feature extraction methods

The different feature extraction techniques tested in this study show markedly different lineament populations that are variably affected by the sharp break in the seafloor. Gradient-based filters are the least effective, despite the initial kernels being selected to emphasise NW and NE gradients, and the Sobel filter underperforms even with smoothing incorporated into the kernel.

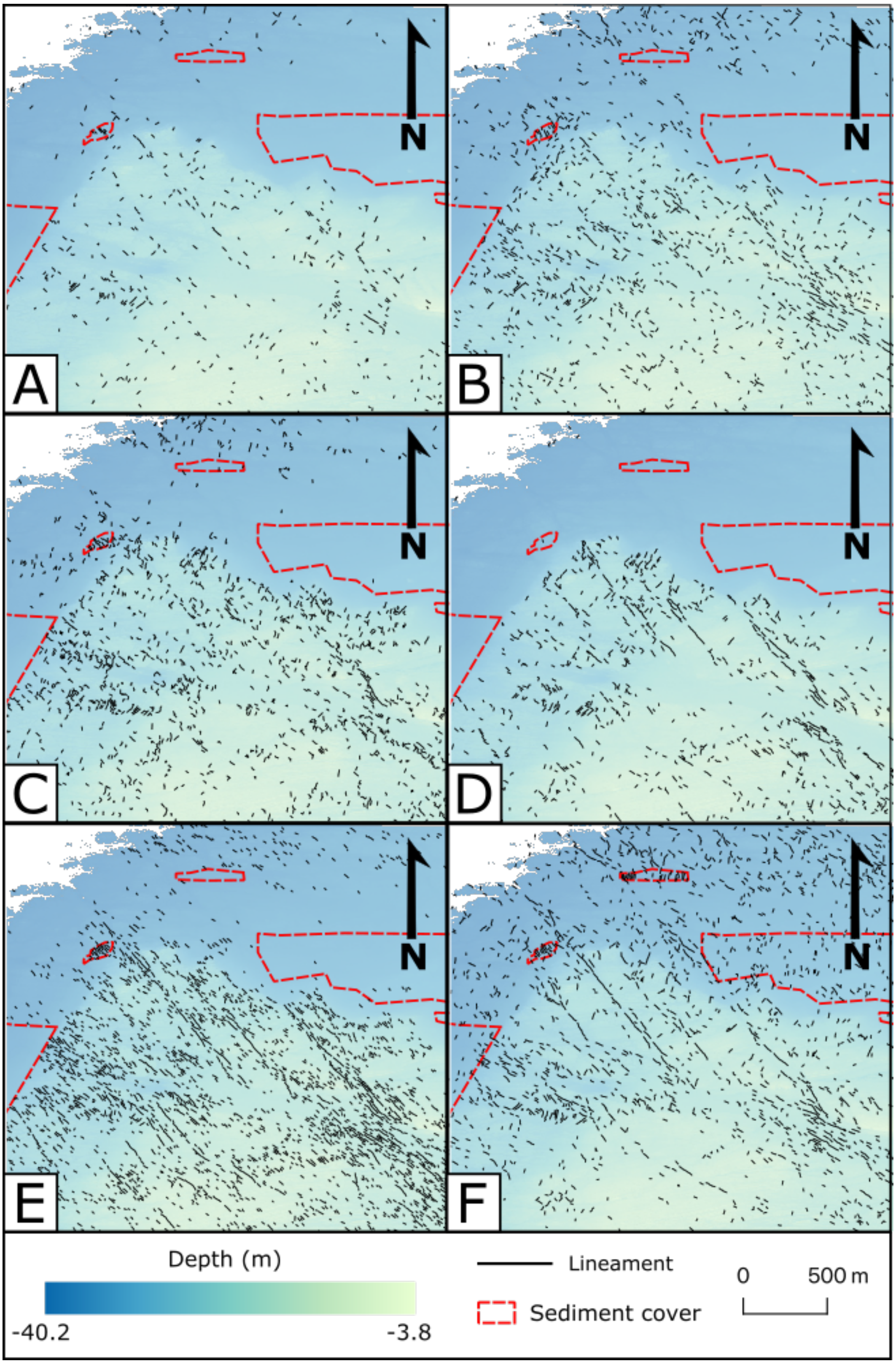

Figure 3. A subset of the lineament populations highlighting performance over the platform edge where the tilt derivative captures the most consistent lineament set. Derived from A) magnitude of gradient filter; B) magnitude of Sobel filter; C) 3 x 3 Laplacian filter; D) 5 x 5 Laplacian filter; E) hillshade transform; F) tilt derivative (TDR) transform.

The Laplacian filters successfully identify structures, albeit discontinuously, with a distinct improvement when using the 5 x 5 kernel. Despite reasonable success on the platform, the filter fails to capture any significant structure in the off-platform area.

Numerous, clear NW-SE lineaments are identified when using the hillshade transform in on-platform areas. Including another hillshade with an orthogonal azimuth (e.g. Scheiber et al., 2015) or taking a multi-hillshade clustering approach (e.g. Šilhavý et al., 2016) would likely further improve this analysis. Unfortunately, off-platform areas do not capture features to the same level of consistency and are not easily interpretable.

Due to the inclusion of the vertical derivative, the TDR transform has provided structures that are consistently identified across the break in seafloor. The transform captures both the NW-SE and subordinate NE-SW fault sets demonstrating azimuth invariance with generally long lineament segments.

Segmented lineaments are common across all analyses and may be a reflection of slight changes in fault properties along strike (e.g. damage zones) that may have preferentially eroded in the seafloor. Thus, post-processing to link these segments should be investigated. Furthermore, the possible detection of amplified noise in some off-platform areas by the TDR transform could be mitigated by prior application of a smoothing filter.

4 Summary

Six different operators have been tested as feature extraction tools prior to semi-automated lineament detection. The different filters and transforms have been assessed based on their performance to detect lineaments from bathymetric data where step-changes (palaeocoastlines) in the seafloor platform are present. These included the magnitude of gradient through combined NW and NE gradient filters, the magnitude of the Sobel filter, two Laplacian filters (3 x 3 and a 5 x 5 kernels) as well as the hillshade and TDR transform.

The bathymetric data used in this study show a network of NW-SE and NE-SW faults sets that can be identified using semi-automated lineament detection techniques. Semi-automated approaches have been demonstrated to produce markedly different lineament populations based on different feature extraction tools. Thus, testing over a small area is an important step prior to using semi-automated methods on regional scale. The semi-automated OBIA lineament detection method of Yeomans et al. (2019) has been applied to bathymetric data to analyse the six operators, of which, the TDR transform was most successful. The algorithm also performed well when applied to the hillshade transform, demonstrating the potential to greatly extend the use of the algorithm to analyse other geospatial datasets.

Ultimately, this study has demonstrated that the use of the TDR transform enhances the data so that abrupt changes in the bathymetry, such as palaeocoastlines, are not detrimental to the analysis. In turn, this increases the area available for interpretation of offshore fault zones. Whilst the resulting lineament population contains longer lineament segments than the other operators, it is worth noting that the TDR transform is not a panacea for lineament detection techniques. For example, subtle noise in the data over sediment-covered areas has been amplified and mapped as lineaments. Careful pre-processing could either remove these areas prior to analysis or lineaments may be masked during post-processing.

Acknowledgments

CMY is funded by a NERC Highlights grant (NE/S003886/1) on the GWatt project. MH is supported by a NERC GW4+ Doctoral Training Partnership studentship from the Natural Environment Research Council (NERC; NE/L002434/1). JJL holds a Vice-Chancellor Scholarship at the University of Exeter. The data used in this study have been sourced from the UK Hydrographic Office and accessed via the Admiralty Marine Data Portal. The British Geological Survey is thanked for making the BGS Geology 625k (DiGMapGB-625) data freely available. Dr Matt Hall is kindly thanked for his insights into some of the nuances of QGIS and color ramps.

References

Airo, M.-L. (2013). *Structural interpretation of airborne geophysical data: examples from Finland* (Tech. Rep.). Espoo: Geologian Tutkimuskeskus (GTK).

Al-Azemi, A. M., & Divi, R. (2017). Extraction of Geological Structural Lineaments in Northern Kuwait Using High Resolution Landsat 8 ETM+ Satellite Images and Edge Enhancement Techniques. *Journal of Engineering Sciences and Information Technology*, *1*(1), 18–35.

Andrews, B. J., Roberts, J. J., Shipton, Z. K., Bigi, S., Tartarello, M. C., & Johnson, G. (2019, apr). How do we see fractures? Quantifying subjective bias in fracture data collection. *Solid Earth*, *10*(2), 487–516. Retrieved from `https://www.solid-earth.net/10/487/2019/` doi: 10.5194/se-10-487-2019

Ault, A. K., Frenzel, M., Reiners, P. W., Woodcock, N. H., & Thomson, S. N. (2016). Record of paleofluid circulation in faults revealed by hematite(U-Th)/He and apatite fission-track dating: An example from Gower Peninsula fault fissures, Wales. *Lithosphere*, *8*(4), 379–385. doi: 10.1130/L522.1

Blaschke, T., Burnett, C., & Pekkarinen, A. (2004). Image Segmentation Methods for Object-based Analysis and Classification. In S. M. de Jong & F. D. van der Meer (Eds.), *Remote sensing image analysis: Including the spatial domain* (pp. 211–236). Springer Netherlands.

Chapman, T. J. (1989). The Permian to Cretaceous structural evolution of the Western Approaches Basin (Melville sub-basin), UK. *Geological Society Special Publication*, *44*(44), 177–200. doi: 10.1144/GSL.SP.1989.044.01.11

Cheadle, M. J., McGeary, S., Warner, M. R., & Matthews, D. H. (1987). Extensional structures on the western UK continental shelf: A review of evidence from deep seismic profiling. *Geological Society Special Publication*, *28*(28), 445–465. doi: 10.1144/GSL.SP.1987.028.01.28

Collier, J. S., Gupta, S., Potter, G., & Palmer-Felgate, A. (2006). Using bathymetry to identify basin inversion structures on the English Channel shelf. *Geology*, *34*(12), 1001. Retrieved from `https://pubs.geoscienceworld.org/geology/article/34/12/1001-1004/129412` doi: 10.1130/G22714A.1

Davies, E. R. (1986). Constraints on the design of template masks for edge detection. *Pattern Recognition Letters*, *4*(2), 111–120. doi: 10.1016/0167-8655(86)90032-2

Fairhead, J. D., Mackenzie, C., Green, C. M., & Verduzco, B. (2004, dec). A new set of magnetic field derivatives for mapping mineral prospects. *ASEG Extended Abstracts*, *2004*(1), 1–4. Retrieved from `https://www.tandfonline.com/doi/full/10.1071/ASEG2004ab042` doi: 10.1071/ASEG2004ab042

Favalli, M., & Fornaciai, A. (2017). Visualization and comparison of DEM-derived parameters. Application to volcanic areas. *Geomorphology*, *290*, 69–84. Retrieved from `http://dx.doi.org/10.1016/j.geomorph.2017.02.029` doi: 10.1016/j.geomorph.2017.02.029

Grebby, S., Cunningham, D., Naden, J., & Tansey, K. (2012). Application of airborne LiDAR data and airborne multispectral imagery to structural mapping of the upper section of the Troodos ophiolite, Cyprus. *International Journal of*

Earth Sciences, *101*, 1645–1660. doi: 10.1007/s00531-011-0742-3

Hell, B., Broman, B., Jakobsson, L., Jakobsson, M., Magnusson, Å., & Wiberg, P. (2012). The use of bathymetric data in society and science: A review from the Baltic Sea. *Ambio*, *41*(2), 138–150. doi: 10.1007/s13280-011-0192-y

Hillis, R. R., Holford, S. P., Green, P. F., Doré, A. G., Gatliff, R. W., Stoker, M. S., ... Williams, G. A. (2008). Cenozoic exhumation of the southern British Isles. *Geology*, *36*(5), 371–374. Retrieved from `https://doi.org/10.1007/s11053-019-09564-8whttp://link.springer.com/10.1007/s11053-019-09564-8` doi: 10.1130/G24699A.1

Höfle, B., & Rutzinger, M. (2011). Topographic airborne LiDAR in geomorphology: A technological perspective. *Zeitschrift fur Geomorphologie*, *55*(March), 1–29. doi: 10.1127/0372-8854/2011/0055S2-0043

Holder, M. T., & Leveridge, B. E. (1986, jan). A model for the tectonic evolution of south Cornwall. *Journal of the Geological Society, London*, *143*(1), 125–134. doi: 10.1144/gsjgs.143.1.0125

Holloway, S., & Chadwick, R. A. (1986). The Sticklepath-Lustleigh fault zone: Tertiary sinistral reactivation of a Variscan dextral strike-slip fault. *Journal of the Geological Society, London*, *143*, 447–452.

Lang, S. (2008). Object-based image analysis for remote sensing application: modeling reality - dealing with complexity. In T. Blaschke, S. Lang, & G. J. Hay (Eds.), *Object-based image analysis: Spatial concepts for knowledge-driven remote sensing applications* (pp. 3–27). Berlin: Springer-Verlag.

Leveridge, B. E., & Hartley, A. J. (2006). The Varisan Orogeny: the development and deformation of Devonian/Carboniferous basins in SW England and South Wales. In P. J. Brenchley & P. F. Rawson (Eds.), *The geology of england and wales* (2nd ed., pp. 225–256). The Geological Society, London.

Leveridge, B. E., Holder, M. T., Goode, A. J. J., Scrivener, R. C., Jones, N. S., & Merriman, R. J. (2002). *Geology of the Plymouth and south-east Cornwall area.* Memoir of the British Geological Survey, Sheet 348. England and Wales.

Lloyd, G. E., & Chinnery, N. (2002). The Bude Formation, SW England - three-dimensional, intra-formational Variscan imbricate stack? *Journal of Structural Geology*, *24*, 1259–1280.

Maini, R., & Aggarwal, H. (2009). Study and comparison of various image edge detection techniques. *International Journal of Image Processing*, *3*(1), 1–11. doi: http://www.doaj.org/doaj?func=openurl&genre=article&issn=19852304&date=2009&volume=3&issue=1&spage=1

Mallast, U., Gloaguen, R., Geyer, S., Rödiger, T., & Siebert, C. (2011). Derivation of groundwater flow-paths based on semi-automatic extraction of lineaments from remote sensing data. *Hydrology and Earth System Sciences*, *15*(8), 2665–2678. doi: 10.5194/hess-15-2665-2011

Marpu, P. R., Niemeyer, I., Nussbaum, S., & Gloaguen, R. (2008). A procedure for automatic object-based classification. In T. Blaschke, S. Lang, & G. J. Hay (Eds.), *Object-based image analysis: Spatial concepts for knowledge-driven remote sensing applications* (pp. 169–184). doi: 10.1007/978-3-540-77058-9

Marr, D., & Hildreth, E. (1980, feb). Theory of edge detection. *Proceedings of the Royal Society of London. Series B. Biological Sciences*, *207*(1167), 187–217. Retrieved from `https://royalsocietypublishing.org/doi/10.1098/rspb.1980.0020` doi: 10.1098/rspb.1980.0020

Mavrantza, O. D., & Argialas, D. P. (2006). Object-oriented image analysis for the identification of geologic lineaments. *International Archives of Photogrammetry, Remote Sensing and Spatial Information Sciences*, *36*(4/C42), 1–6.

Middleton, M., Schnur, T., Sorjonen-ward, P., & Hyvönen, E. (2015). Geological lineament interpretation using the Object-Based Image Analysis Approach: results of semi-automated analyses versus visual interpretation. *Geological Survey of Finland, Special Paper*, *57*, 135–154.

Miller, H. G., & Singh, V. (1994). Potential field tilt - a new concept for location of potential field sources. *Journal of Applied Geophysics*, *32*(2-3), 213–217. doi: 10.1016/0926-9851(94)90022-1

Moore, G. K., & Waltz, F. A. (1983). Objective procedures for lineament enhancement and extraction (Eros Data Center). *Photogrammetric Engineering & Remote Sensing*, *49*(5), 641–647.

Nixon, C. W., Sanderson, D. J., & Bull, J. M. (2012, may). Analysis of a strike-slip fault network using high resolution multibeam bathymetry, offshore NW Devon U.K. *Tectonophysics*, *541-543*, 69–80. Retrieved from `http://dx.doi.org/10.1016/j.tecto.2012.03.021` doi: 10.1016/j.tecto.2012.03.021

Nyberg, B., Nixon, C. W., & Sanderson, D. J. (2018). NetworkGT: A GIS tool for geometric and topological analysis of two-dimensional fracture networks. *Geosphere*, *14*(4), 1618–1634. doi: 10.1130/GES01595.1

Rahnama, M., & Gloaguen, R. (2014, jun). TecLines: A MATLAB-Based Toolbox for Tectonic Lineament Analysis from Satellite Images and DEMs, Part 1: Line Segment Detection and Extraction. *Remote Sensing*, *6*(7), 5938–5958. Retrieved from `http://www.mdpi.com/2072-4292/6/7/5938` doi: 10.3390/rs6075938

Rattey, P. R., & Sanderson, D. J. (1984). The structure of SW Cornwall and its bearing on the emplacement of the Lizard Complex. *Journal of the Geological Society, London*, *141*, 87–95.

Rutzinger, M., Höfle, B., Pfeifer, N., Geist, T., & Stötter, H. (2006). Object based analysis of airborne laser scanning data for natural hazard purposes using open source components. In *1st international conference on object-based image analysis* (p. 5).

Sanderson, D. J., Dix, J. K., Westhead, K. R., & Collier, J. S. (2017, may). Bathymetric mapping of the coastal and offshore geology and structure of the Jurassic Coast, Weymouth Bay, UK. *Journal of the Geological Society*, *174*(3), 498–508. Retrieved from `http://jgs.lyellcollection.org/lookup/doi/10.1144/jgs2016-070` doi: 10.1144/jgs2016-070

Scheiber, T., Fredin, O., Viola, G., Jarna, A., Gasser, D., & Łapińska-Viola, R. (2015). Manual extraction of bedrock lineaments from high-resolution LiDAR data: methodological bias and human perception. *Journal of the Geological Society of Sweden (GFF)*, *137*(4), 362–372. doi: 10.1080/11035897.2015.1085434

Sedrette, S., & Rebaï, N. (2016). Automatic extraction of lineaments from Landsat Etm+ images and their structural interpretation: Case Study in Nefza region (North West of Tunisia). *Journal of Research in Enviromental and Earth Sciences*, *04*, 139–145.

Shail, R. K., & Alexander, A. C. (1997, feb). Late Carboniferous to Triassic reactivation of Variscan basement in the western English Channel: evidence from onshore exposures in south Cornwall. *Journal of the Geological Society, London*, *154*(1), 163–168. doi: 10.1144/gsjgs.154.1.0163

Šilhavý, J., Minár, J., Mentlík, P., & Sládek, J. (2016). A new artefacts resistant method for automatic lineament extraction using Multi-Hillshade Hierarchic Clustering (MHHC). *Computers & Geosciences*, *92*, 9–20.

Smith, M. J., & Clark, C. D. (2005). Methods for the visualization of digital elevation models for landform mapping. *Earth Surface Processes and Landforms*, *30*(7), 885–900. doi: 10.1002/esp.1210

Sobel, I., & Feldman, G. (1973). A 3x3 Isotropic Gradient Operator for Image Processing. *Pattern Classification and Scene Anlaysis*, 271–272.

Sukumar, M., Venkatesan, N., & Babu, C. N. K. (2014). A review of various lineament detection techniques for high resolution satellite images. *International Journal of Advanced Research in Computer Science and Software Engineering*, *4*(3), 72–78.

Van Den Eeckhaut, M., Kerle, N., Poesen, J., & Hervás, J. (2012). Object-oriented identification of forested landslides with derivatives of single pulse LiDAR data. *Geomorphology*, *173-174*, 30–42. Retrieved from http://dx.doi.org/10.1016/j.geomorph.2012.05.024 doi: 10.1016/j.geomorph.2012.05.024

Van Den Eeckhaut, M., Poesen, J., Verstraeten, G., Vanacker, V., Moeyersons, J., Nyssen, J., & van Beek, L. P. (2005). The effectiveness of hillshade maps and expert knowledge in mapping old deep-seated landslides. *Geomorphology*, *67*(3-4), 351–363. doi: 10.1016/j.geomorph.2004.11.001

Verduzco, B., Fairhead, D., Green, C. M., & MacKenzie, C. (2004). New insights into magnetic derivatives for structural mapping. *The Meter Reader*, 116–119.

Westhead, R. K., McCarthy, D. J., Collier, J. S., & Sanderson, D. J. (2018). Spatial variability of the Purbeck–Wight Fault Zone—a long-lived tectonic element in the southern UK. *Proceedings of the Geologists' Association*, *129*(3), 436–451. Retrieved from http://dx.doi.org/10.1016/j.pgeola.2017.08.005 doi: 10.1016/j.pgeola.2017.08.005

Yeomans, C. M., Middleton, M., Shail, R. K., Grebby, S., & Lusty, P. A. J. (2019, feb). Integrated Object-Based Image Analysis for semi-automated geological lineament detection in southwest England. *Computers & Geosciences*, *123*, 137–148 [Available Online November 2018]. Retrieved from https://doi.org/10.1016/j.cageo.2018.11.005 doi: 10.1016/j.cageo.2018.11.005